One- and Two-Triplon Spectra of a Cuprate Ladder

S. Notbohm,[1,2] P. Ribeiro,[3] B. Lake,[1,4] D. A. Tennant,[1,4] K. P. Schmidt,[5] G. S. Uhrig,[6] C. Hess,[3] R. Klingeler,[3] G. Behr,[3] B. Büchner,[3] M. Reehuis,[1,7] R. I. Bewley,[8] C. D. Frost,[8] P. Manuel,[8] and R. S. Eccleston[9]

[1]*Hahn-Meitner-Institut Berlin, Glienicker Straße 100, 14109 Berlin, Germany*
[2]*School of Physics and Astronomy, University of St. Andrews, St. Andrews, Fife KY16 9SS, United Kingdom*
[3]*Leibniz-Institut for Solid State and Material Research, IFW-Dresden, 01171 Dresden, Germany*
[4]*Institut für Festkörperphysik, Technische Universität Berlin, Hardenbergstraße 36, 10623 Berlin, Germany*
[5]*Institute of Theorectical Physics, École Polytechnique Fédérale de Lausanne, 1015 Lausanne, Switzerland*
[6]*Lehrstuhl für Theoretische Physik I, Universität Dortmund, 44221 Dortmund, Germany*
[7]*Max-Planck-Institut für Festkörperforschung, 70569 Stuttgart, Germany*
[8]*ISIS Facility, Rutherford Appleton Laboratory, Chilton, Didcot OX11 OQX, United Kingdom*
[9]*Materials and Engineering Research Institute, Sheffield Hallam University, Howard Street, Sheffield S1 1WB, United Kingdom*

(Received 13 March 2006; published 12 January 2007)

We have performed inelastic neutron scattering on the near ideal spin-ladder compound $La_4Sr_{10}Cu_{24}O_{41}$ as a starting point for investigating doped ladders and their tendency toward superconductivity. A key feature was the separation of one-triplon and two-triplon scattering. Two-triplon scattering is observed quantitatively for the first time and so access is realized to the important strong magnetic quantum fluctuations. The spin gap is found to be 26.4 ± 0.3 meV. The data are successfully modeled using the continuous unitary transformation method, and the exchange constants are determined by fitting to be $J_{\text{leg}} = 186$ meV and $J_{\text{rung}} = 124$ meV along the leg and rung, respectively; a substantial cyclic exchange of $J_{\text{cyc}} = 31$ meV is confirmed.

DOI: 10.1103/PhysRevLett.98.027403 PACS numbers: 78.70.Nx, 75.10.Jm, 75.30.Ds, 75.30.Et

Cuprate high-T_c superconductors are dominated by strong quantum fluctuations; e.g., magnetic long range order is suppressed on doping the insulating parent compounds. Hence a quantitative understanding of magnetically disordered Heisenberg systems is indispensable. The workhorse of such systems is the two-leg ladder, consisting of two spin-1/2 chains coupled by a Heisenberg interaction. The immediate effect of coupling is to confine pairs of spin-1/2 spinons and to generate a gapped spin singlet ground state. Short ranged singlet pairings on the rungs $1/\sqrt{2}\{|\uparrow\downarrow\rangle - |\downarrow\uparrow\rangle\}$ dominate the ground state, and in an inelastic neutron scattering measurement a triplet of well-defined spin-1 magnons, known as triplon [1] excitations, rather than a spinon pair continuum will appear. Further, strong higher-order ground state fluctuations should manifest as multitriplon continua. The spin pairings are particularly important as they provide a mechanism for the formation of charged hole pairs when doped, giving rise to charge density wave (CDW) or superconducting states [2–5].

Cuprate spin ladders share many features of the 2D high-T_c materials (pseudogap, non-Fermi liquid behavior) [6–8] and have similar coupling parameters. Their excitation spectra extend to several hundred meV, and the development of time-of-flight spectroscopy at spallation neutron sources allows access to the full spectra resolved in wave vector and energy for the first time. Motivated by this, we have measured the one- and two-triplon spectra of a cuprate ladder in a Mott-Hubbard insulating phase—$La_4Sr_{10}Cu_{24}O_{41}$—using inelastic neutron scattering (INS). A full description of the dynamics is achieved using the continuous unitary transformation (CUT) method. Electrostatic environments of the oxygen tunneling result in strongly dissimilar rung and leg exchanges, and this combined with substantial cyclic charge fluctuations render the magnetic state of the system near quantum critical (gapless).

The geometry of cuprate ladders in $La_4Sr_{10}Cu_{24}O_{41}$ is depicted in Fig. 1. Strong antiferromagnetic superexchange occurs through 180° Cu-O-Cu bonds with very weak exchange between ladders via the 90° bonds. An approximate electronic Hamiltonian is the one-band Hubbard model

$$H = -\sum_{\langle i,j\rangle\sigma=\uparrow,\downarrow} t_{i,j}(c^{+}_{i,\sigma}c_{j,\sigma} + \text{H.c.}) + U\sum_{i} n_{i,\uparrow}n_{i,\downarrow} \qquad (1)$$

with on-site Coulomb energy $U \sim 3.5$ eV, intersite hopping between nearest neighbor pairs of $t \sim 0.3$ eV, and $\kappa \equiv t/U \sim \frac{1}{12}$ [9]. Charge fluctuations such as cyclic hopping processes (suppressed for $\kappa \to 0$) modify the Heisenberg spin Hamiltonian by contributing a four-spin interaction term. Computations [10] including O2p and Cu3d orbitals indicate that only short-range Heisenberg and four-spin interactions are important with diagonal coupling across the CuO square plaquette and further neighbor interactions negligible. Hence the Hamiltonian reads

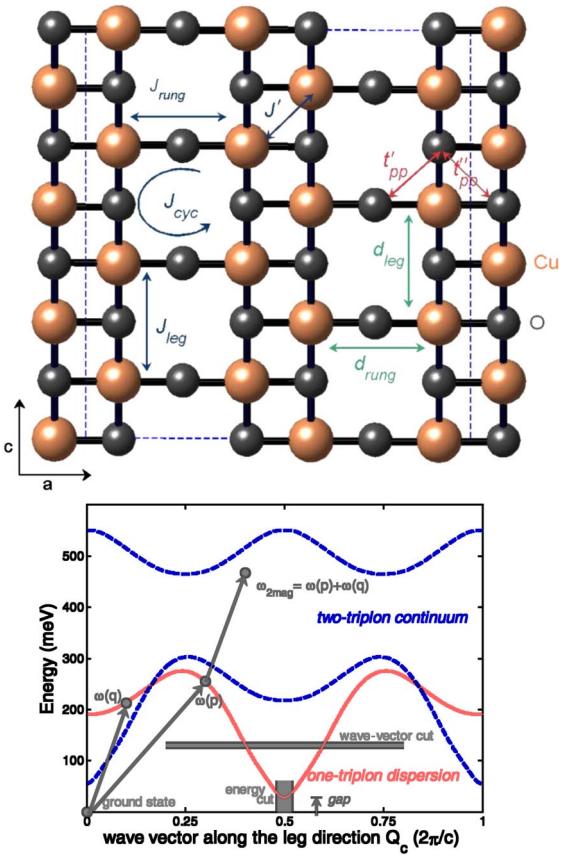

FIG. 1 (color online). Upper part: Arrangement of ladder planes in $La_4Sr_{10}Cu_{24}O_{41}$. Big spheres represent the copper ions, small spheres oxygen atoms. The dashed rectangle displays unit cell in the (010) crystallographic plane for the a axis and half the unit cell in the c axis. Lower part: $S = 1$ excitation spectrum. Gap from the $S = 0$ ground state to the $S = 1$ triplon band (red solid curve). Two-triplon continuum states bounded by the two blue dashed curves can be constructed via the scattering of the two triplons illustrated by the arrows. Typical wave-vector (horizontal) and energy (vertical) cuts are indicated.

$$H = J_{\text{rung}} \sum_i \mathbf{S}_{i,1} \cdot \mathbf{S}_{i,2} + J_{\text{leg}} \sum_{i,\tau} \mathbf{S}_{i,\tau} \cdot \mathbf{S}_{i+1,\tau} + H_{\text{cyc}},$$

$$H_{\text{cyc}} = J_{\text{cyc}} \sum_{\text{plaquettes}} [(\mathbf{S}_{i,1} \cdot \mathbf{S}_{i+1,1})(\mathbf{S}_{i,2} \cdot \mathbf{S}_{i+1,2}) + (\mathbf{S}_{i,1} \cdot \mathbf{S}_{i,2})(\mathbf{S}_{i+1,1} \cdot \mathbf{S}_{i+1,2}) - (\mathbf{S}_{i,1} \cdot \mathbf{S}_{i+1,2})(\mathbf{S}_{i+1,1} \cdot \mathbf{S}_{i,2})]. \quad (2)$$

The anticipated dispersion relation for the spin-1 triplon states (as predicted by the CUT) is plotted in the lower part of Fig. 1. The ratios of the gaps along the leg direction $Q_c = 0$, 0.25, and 0.5 (in units of $2\pi/c$) are modified substantially by the strength of J_{cyc}.

Also shown are the boundaries of the two-triplon continuum. The intensity of the two-triplon spectrum, wave vector, and energy distribution depends strongly on the triplon interactions, the matrix elements, and the exact composition of the ground state. Importantly, a bound spin-1 state is predicted below the two-triplon continuum. The four-spin exchange term frustrates the formation of this bound mode lowering the binding energy and for coupling strengths of order $x_{\text{cyc}} = J_{\text{cyc}}/J_{\text{rung}} \sim 0.25$ will disrupt binding completely.

A remarkable property of the undoped ladder geometry is that the sectors of even and odd triplon number do not mix because of different parity with respect to reflection about the centerline of the ladder. Hence even and odd contributions can be Fourier decomposed by the rung coupling, and the neutron scattering matrix elements can be expressed as a product of a neutron structure factor (NSF) dependent only on the wave vector along the leg direction q_c, multiplied by a rung wave-vector q_a modulation. The one- and two-triplon spectra are in antiphase with rung modulations $[1 - \cos(qa)]$ and $[1 + \cos(qa)]$, respectively [11], and this can be used to separate them.

Here we investigate $La_4Sr_{10}Cu_{24}O_{41}$: Although intrinsically hole doped, x-ray absorption spectroscopy reveals for the substitution of La in $Sr_{14}Cu_{24}O_{41}$ that residual holes are located in the more electronegative chains [12], leaving ladders undoped [13]. No triplon-hole scattering is observed in the heat conductivity [14].

Large $La_4Sr_{10}Cu_{24}O_{41}$ single crystals were prepared using the "traveling solvent floating zone" method at 9 bar oxygen pressure. INS measurements were performed using the MAPS spectrometer at ISIS, U.K. Three crystals totaling 23 g were coaligned with a resulting mosaic spread of 0.4° in the b-c plane and 5.5° in the a-c plane. The samples were mounted with the b-c plane horizontal and the c axis (leg direction) perpendicular to the incident neutron wave vector k_i; a cryostat provided a temperature of 10 K. The wave vectors are labeled Q_c along the leg and Q_a along the rung. The magnetic cross section was normalized using incoherent nuclear scattering from a vanadium standard. Data were collected for incident energies $E_i = 75.55$, 363.7, and 606.2 meV using a Fermi chopper at 300 Hz for the low energy run and at 600 Hz for the other runs.

Contributions mainly from one-triplon or two-triplon scattering were separated using the antiphase rung modulation. The measured modulation is shown in Fig. 2(a) with the one-triplon modulation fitted to $[1 - \cos(qa)]$ and the two-triplon modulation to $[1 + \cos(qa)]$, with corrections for the anisotropic magnetic form factor of copper [15] applied to the fitted functions. One-triplon data used in subsequent analysis were taken at the maxima between $1 < |Q_a| < 2$; see in Fig. 2(a). For the two-triplon data, two regions of maximum two-triplon intensity $0 < |Q_a| < 0.5$ and $2.65 < |Q_a| < 3.35$ were added taking magnetic form factor corrections fully into account.

The nonmagnetic background for the one-triplon signal was deduced via interpolation of the intensity found at energies above and below the one-triplon dispersion. The background subtracted data are displayed in Fig. 3(a). Figure 3(c) shows two-triplon scattering minus background deduced at $Q_c = 0$, 1, and 2 where magnetic signal is weak.

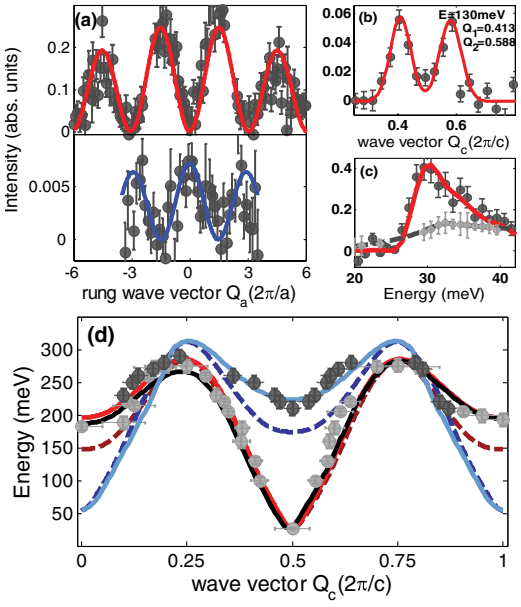

FIG. 2 (color). (a) Cut along the rung wave vector shows the intensity modulation. Upper part: one-triplon scattering. Cut for energy of 30 ± 5 meV and leg wave vector of 0.45 ± 0.05 in the rung direction. Lower part: two-triplon cut for energy of 300 ± 10 meV and leg wave vector of 0.25 ± 0.05. Solid line described in text. (b) Typical wave-vector cut through one-triplon along Q_c for energy of 130 ± 5 meV. The solid line is a Gaussian fit to extract peak position. (c) Energy cut for $0.48 < Q_c < 0.52$ to determine the energy gap. Light gray points are the corresponding cut for a hole-doped ladder. (d) Experimental points from neutron data. Theoretical one-triplon dispersion curves shown by solid red and black curves. Black curve includes interladder coupling. Theoretical lower boundary of two-triplon scattering shown by solid blue curve. Dashed lines show respective scattering without cyclic exchange.

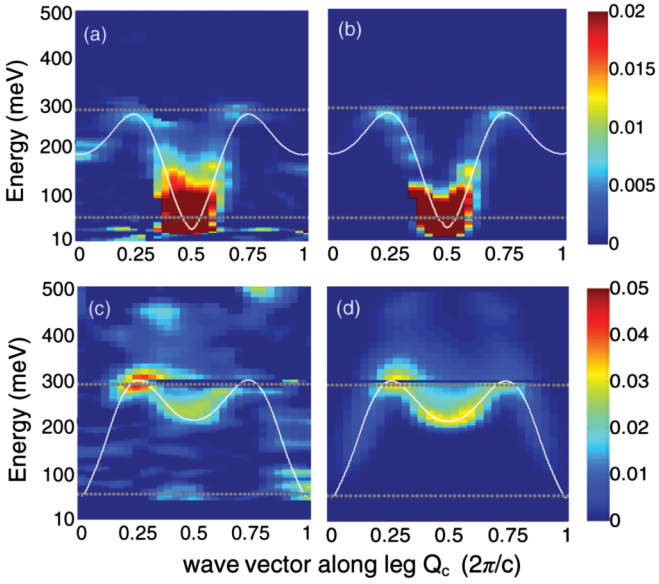

FIG. 3 (color). (a) Measured one-triplon data with nonmagnetic background subtracted. The white curve gives the theoretically calculated one-triplon dispersion curve. (b) Calculated one-triplon scattering with corrections for instrumental resolution and magnetic form factor. (c) Measured two-triplon data with nonmagnetic background subtracted. The white curve gives the lower boundary of the two-triplon dispersion curve. (d) Calculated two-triplon scattering.

The one-triplon dispersion was determined from the positions and intensities of measured peaks by least-squares fitting of Gaussians. A typical cut is shown in Fig. 2(b) giving Q_c at energy of 130 ± 5 meV indicated in Fig. 1 by the horizontal slice. These along with data points from different cuts are displayed in Fig. 2(d). Heisenberg couplings alone are unable to account for the energy gaps of 197, 286, and 26.4 meV, at wave vectors 0, 0.25, and 0.5, respectively. Our computations based on CUTs [11] reveal that a substantial four-spin coupling $J_{\mathrm{cyc}} = 31$ meV and Heisenberg couplings along the legs $J_{\mathrm{leg}} = 186$ meV and rungs $J_{\mathrm{rung}} = 124$ meV are required to explain this. Qualitatively, this agrees with previous analyses of optical data [16,17] but deviates from previous INS results [18] $J_{\mathrm{leg}} = J_{\mathrm{rung}} = 110$ meV and $J_{\mathrm{cyc}} = 33$ meV as far as $J_{\mathrm{leg}}/J_{\mathrm{rung}}$ is concerned. Using these values, the entire theoretical dispersion (solid red line) agrees excellently with the data [19]. The lower boundary of the two-triplon scattering was extracted in the same manner and is plotted in Fig. 2(d). Also shown are the computed dispersions in the absence of cyclic exchange (dashed curves). One can see the necessity of the cyclic exchange to describe the data within error bars.

The CUT method is also used to compute the NSF, which agrees very well with the measured scattering; see Figs. 3(b) and 3(d). A complete simulation of detector coverage and multicrystal mount is included with the detailed angular mosaics of each crystal, measured via neutron Laue, accounted for using a Monte Carlo integration. The uneven intensity profile of the data with wave vector is due to a combination of detector coverage and crystalline mosaic. Figure 2(c) shows an energy cut at $Q_c = 0.5$ (vertical slice in Fig. 1, wave-vector range $0.48 < |Q_c| < 0.52$). The computed NSF including instrumental corrections is shown as the red line and matches the data. Note the fitted gap is 26.4 ± 0.3 meV, which is lower than found in previous measurements [20,21].

The effect of cyclic exchange on the two-triplon binding is illustrated in Fig. 4. The data points in Fig. 4(a) show a two-triplon energy cut at $Q_c = 0.5 \pm 0.1$; the red solid line is the same cut computed for the model with the determined couplings. Figure 4(b) illustrates the dependence of the continuum onset energy ω_{onset} (measured as 224 meV), with J_{rung} determined to match the one-triplon gaps at $Q_c = 0.25$ and 0.5, on cyclic exchange ratio $x_{\mathrm{cyc}} \equiv J_{\mathrm{cyc}}/J_{\mathrm{rung}}$. Keeping J_{rung} fixed and assuming no cyclic exchange, a bound mode 12 meV below ω_{onset} would appear, shown in Fig. 4(c) $\omega_{\mathrm{binding}} = 12$ meV. Such a shift is indicated by the black dashed line in Fig. 4(a) and would be detectable within our resolution limits, confirming we

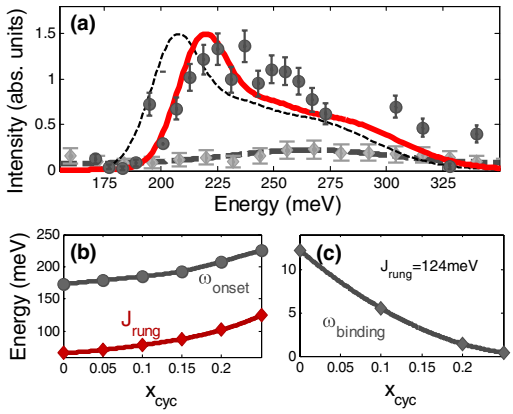

FIG. 4 (color online). (a) Energy cut for two triplon at $Q_c = 0.5 \pm 0.1$. The solid line is the two-triplon model. Intensities had to be increased by 15% to match data. Light gray points are the corresponding cut for a hole-doped ladder. The thin dashed line is the effect of absent cyclic exchange for fixed J_{rung}. (b) Relationship of ω_{onset} and J_{rung} with respect to x_{cyc}. For an onset energy of 225 meV, $J_{\text{rung}} = 124$ meV and $x_{\text{cyc}} = 0.25$ are needed (see text). $J_{\text{cyc}} = x_{\text{cyc}} J_{\text{rung}}$. (c) Frustration of bound mode by cyclic exchange. Binding energy ω_{binding} is the difference between ω_{onset} and energy of the bound mode.

are on the binding threshold. van Hove singularities in phonon assisted IR absorption measurements indicate that $S = 0$ bound states survive as they are more stable in quantum antiferromagnets [11,16,22].

Figures 3(c) and 3(d) show that nearly all the $S = 1$ two-triplon scattering weight is concentrated near the lower continuum boundary, as is reproduced very well by calculation. The CUT method also predicts the relative one- and two-triplon neutron scattering intensity scales. The scale factors applied to the model above are within 15% of the computations, i.e., within experimental accuracy.

Approximate parameters for (1), $t_{\text{leg}} = 0.42$, $t_{\text{rung}} = 0.34$, and $U = 3.72$ eV, follow from low order perturbation theory [23], but recourse to 3-band computations is necessary for high accuracy. The large difference between rung and leg exchange implies stronger hopping along the legs $t_{\text{leg}} > t_{\text{rung}}$ despite a longer pathway ($d_{\text{leg}} = 3.96$ Å, $d_{\text{rung}} = 3.84$ Å). Contributions from hopping between O2p orbitals [24] depend acutely on the electrostatic environment [25]. For ladders (Fig. 1), O2p hopping along the leg, t''_{pp} is enhanced by two neighboring Cu^{2+} ions compared to the rung, t'_{pp} which has one Cu^{2+} neighbor [25] accounting for the stronger t_{leg}. Further, admixture of Cu4s states has been proposed to enhance t_{leg} (by 35%) [26,27] compared to t_{rung}. Comparison of our J_{leg}, J_{rung}, and J_{cyc} with theoretical calculation should lead to a more refined model for cuprate electronic structure.

For doped $Sr_{2.5}Ca_{11.5}Cu_{24}O_{41}$, results are obtained for where the ladder has a modest doping of 5% holes ($\rho \propto T$ above $T_{\text{CDW}} \sim 80$ K). Our MAPS measurements show the one-triplon spectra to split into multiple branches and for the gap to develop into a pseudogap [see Fig. 2(c)]. Further, the holes break the parity conservation which is reflected in additional scattering in the two-magnon channel around $Q_c = 0.5$ [see Fig. 4(a)]. Understanding these findings quantitatively will provide significant progress in the analysis of high-T_c superconductivity.

In summary, our new INS measurements determine the full one- and two-triplon spectra in an insulating cuprate ladder quantitatively. In particular, the two-triplon part marks a major breakthrough because it represents the signature of strong quantum fluctuations which govern also the physics of high-T_c superconductors. Furthermore, a fingerprint of strong triplon-triplon interaction has been found. All experimental data agreed accurately with the theoretical results from the continuous unitary transformation method. Computations and further measurements for doped Mott insulators are urgently needed.

We thank T. G. Perring, H.-J. Mikeska, A. L. Läuchli, and S.-L. Drechsler for discussion and the Deutsche Forschungsgemeinschaft for Grant No. UL 164/4.

[1] K. P. Schmidt *et al.*, Phys. Rev. Lett. **90**, 227204 (2003).
[2] E. Dagotto *et al.*, Phys. Rev. B **45**, 5744 (1992).
[3] T. M. Rice *et al.*, Europhys. Lett. **23**, 445 (1993).
[4] S. Gopalan, T. M. Rice, and M. Sigrist, Phys. Rev. B **49**, 8901 (1994).
[5] M. Troyer, H. Tsunetsugu, and T. M. Rice, Phys. Rev. B **53**, 251 (1996).
[6] M. Takahashi *et al.*, Physica (Amsterdam) **237B–238B**, 112 (1997).
[7] E. Dagotto, Rep. Prog. Phys. **62**, 1525 (1999).
[8] J. M. Tranquada *et al.*, Nature (London) **429**, 534 (2004).
[9] K.-Y. Yang *et al.*, cond-mat/0603423.
[10] E. Müller-Hartmann and A. Reischl, Eur. Phys. J. B **28**, 173 (2002).
[11] K. P. Schmidt and G. S. Uhrig, Mod. Phys. Lett. B **19**, 1179 (2005).
[12] N. Nücker *et al.*, Phys. Rev. B **62**, 14 384 (2000).
[13] S. A. Carter *et al.*, Phys. Rev. Lett. **77**, 1378 (1996).
[14] C. Hess *et al.*, Phys. Rev. Lett. **93**, 027005 (2004).
[15] S. Shamoto *et al.*, Phys. Rev. B **48**, 13 817 (1993).
[16] T. Nunner *et al.*, Phys. Rev. B **66**, 180404(R) (2002).
[17] K. P. Schmidt *et al.*, Phys. Rev. B **72**, 094419 (2005).
[18] M. Matsuda *et al.*, Phys. Rev. B **62**, 8903 (2000).
[19] We also explored interladder effects within the RPA. The black line in Fig. 2(d) is the dispersion computed including an interchain exchange $J' = 36$ meV. The interladder coupling does not have a large effect on the dispersion and is undetermined with experimental accuracy.
[20] R. S. Eccleston *et al.*, Phys. Rev. B **53**, R14721 (1996).
[21] M. Azuma *et al.*, Phys. Rev. Lett. **73**, 3463 (1994).
[22] M. Windt *et al.*, Phys. Rev. Lett. **87**, 127002 (2001).
[23] Parameters to $\mathcal{O}(\kappa^4)$: $J_{\text{leg}} = 4t_{\text{leg}}^2/U$, $J_{\text{rung}} = 4t_{\text{rung}}^2/U$, and $J_{\text{cyc}} = 80 t_{\text{leg}}^2 t_{\text{rung}}^2/U^3$.
[24] H. Eskes and J. H. Jefferson, Phys. Rev. B **48**, 9788 (1993).
[25] Y. Mizuno *et al.*, Phys. Rev. B **58**, R14713 (1998).
[26] M. Arai and H. Tsunetsugu, Phys. Rev. B **56**, R4305 (1997).
[27] T. F. A. Müller *et al.*, Phys. Rev. B **57**, R12655 (1998).